Chapman University
Chapman University Digital Commons

Biology, Chemistry, and Environmental Sciences Faculty Articles and Research

Biology, Chemistry, and Environmental Sciences

3-2015

Influence of Microgel Packing on Raspberry-Like Heteroaggregate Assembly

Shalini Saxena
Georgia Institute of Technology

L. Andrew Lyon
Chapman University, lyon@chapman.edu

Follow this and additional works at: http://digitalcommons.chapman.edu/sees_articles

 Part of the Chemistry Commons, and the Physics Commons

Recommended Citation
Shalini Saxena, L. Andrew Lyon. Influence of Microgel Packing on Raspberry-Like Heteroaggregate Assembly, *Journal of Colloid and Interface Science*, March 2015. doi: 10.1016/j.jcis.2014.11.033.

This Article is brought to you for free and open access by the Biology, Chemistry, and Environmental Sciences at Chapman University Digital Commons. It has been accepted for inclusion in Biology, Chemistry, and Environmental Sciences Faculty Articles and Research by an authorized administrator of Chapman University Digital Commons. For more information, please contact laughtin@chapman.edu.

Influence of Microgel Packing on Raspberry-Like Heteroaggregate Assembly

Comments
NOTICE: this is the author's version of a work that was accepted for publication in *Journal of Colloid and Interface Science*, volume 442, in 2015. Changes resulting from the publishing process, such as peer review, editing, corrections, structural formatting, and other quality control mechanisms may not be reflected in this document. Changes may have been made to this work since it was submitted for publication. A definitive version was published at the following address: DOI: 10.1016/j.jcis.2014.11.033

The Creative Commons license below applies only to this version of the article.

Creative Commons License

This work is licensed under a Creative Commons Attribution-Noncommercial-No Derivative Works 4.0 License.

Copyright
Elsevier

This article is available at Chapman University Digital Commons: http://digitalcommons.chapman.edu/sees_articles/1

Accepted Manuscript

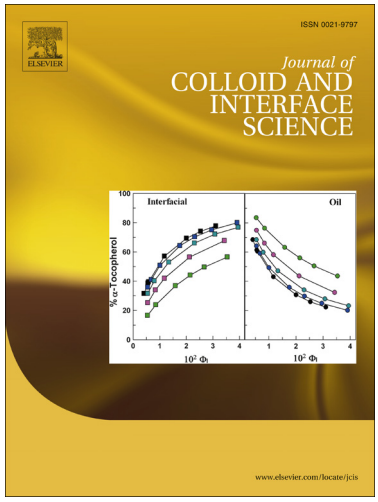

Influence of Microgel Packing on Raspberry-Like Heteroaggregate Assembly

Shalini Saxena, L. Andrew Lyon

PII: S0021-9797(14)00881-9
DOI: http://dx.doi.org/10.1016/j.jcis.2014.11.033
Reference: YJCIS 20000

To appear in: *Journal of Colloid and Interface Science*

Received Date: 20 September 2014
Accepted Date: 14 November 2014

Please cite this article as: S. Saxena, L. Andrew Lyon, Influence of Microgel Packing on Raspberry-Like Heteroaggregate Assembly, *Journal of Colloid and Interface Science* (2014), doi: http://dx.doi.org/10.1016/j.jcis.2014.11.033

This is a PDF file of an unedited manuscript that has been accepted for publication. As a service to our customers we are providing this early version of the manuscript. The manuscript will undergo copyediting, typesetting, and review of the resulting proof before it is published in its final form. Please note that during the production process errors may be discovered which could affect the content, and all legal disclaimers that apply to the journal pertain.

ACCEPTED MANUSCRIPT

Influence of Microgel Packing on Raspberry-Like Heteroaggregate Assembly

*Shalini Saxena[1,2] and L. Andrew Lyon[2,3,4]**

1. School of Materials Science and Engineering, Georgia Institute of Technology, Atlanta, GA 30332, United States of America
2. Petit Institute for Biosciences and Bioengineering, Georgia Institute of Technology, Atlanta, GA 30332, United States of America
3. School of Chemistry and Biochemistry, Georgia Institute of Technology, Atlanta, GA 30332, United States of America
4. Schmid College of Science and Technology, Chapman University, Orange, CA 92866, United States of America

*Corresponding Author
Shalini Saxena
Email: ssaxena30@gatech.edu

L. Andrew Lyon
Email: lyon@chapman.edu
Telephone: 714-997-6930
Fax: 714-532-6048

Abstract

We describe the influence of microgel packing on colloidal-phase mediated heteroaggregation using poly(*N*-isopropylacrylamide) and poly(*N*-isopropylmethacrylamide) microgels with 1% mol or 5% mol *N,N'*-methylenebis(acrylamide) cross-linker. This system is uniquely designed to interrogate the influence of microgel structure and stiffness on microgel deformation at a curved interface by elminating the necessity of electrostatic charge pairing. Microgel monomer and cross-linker content is expected to influence deformation at a curved interface. Microgel deformation and swelling were characterized via atomic force microscopy (AFM) and viscometry. A systematic study of colloidal-phase heteroaggregation was performed at varied effective volume fractions with all microgel compositions. Scanning electron microscopy (SEM) and qNano pore translocation experiments are used to asses the microgel coverage on the resultant raspberry-like particles (RLPs). Results reveal that microgel composition has a strong influence on the efficiency (as determined by microgel coverage) of RLP fabrication. The compositional effects appear to be related to the degree of microgel spreading/deformation at the interface, which is coupled to the influence of packing on assembly fidelity. These findings are widely applicable to systems where microgel deformation occurs at a curved interface. We also demonstrate that qNano pore translocation experiments can be used as a high-throughput method to analyze RLP microgel coverage.

Keywords: heteroaggregation, core-shell microparticles, microgel network strutures

ACCEPTED MANUSCRIPT

Abbreviations

Atomic Force Microscopy	AFM
Raspberry-Like Particles	RLPs
Scanning Electron Microscopy	SEM
Effective Volume Fraction	ϕ_{eff}
Volume Phase Transition Temperature	VPTT
N-isoproprylacrylamide	NIPAm
Poly(*N*-isoproprylacrylamide)	pNIPAm
N-isoproprylmethacrylamide	NIPMAm
Poly*(N*-isoproprylmethacrylamide)	pNIPMAm
N,N'-methylenebis(acrylamide)	BIS
Acrylic Acid	Aac
Sodium Dodecyl Sulfate	SDS
Ammonium Persulfate	APS
1-ethyl-2-[2-dimethylaminopropyl]carbodiimide hydrochloride	EDC
N-hydroxysuccinimide	NHS
4-Aminobenzophenone	AB
Ethanol	EtOH
Dimethylsulfoxide	DMSO
Polystyrene	PS
Phosphate Buffer Solution	PBS

1. Introduction

ACCEPTED MANUSCRIPT

Recently, architectural control of composite nano- and microparticles has gained importance in the development of functional materials. The creation of multi-material colloidal particles (i.e. polymer/polymer,[1] polymer/metal,[2] polymer/mineral,[3] mineral/metal,[4] metal/metal,[5] etc.) can lead to complex properties that are not simple compositional averages of the individual materials, with those properties being tunable to meet specific needs of an application. Previous studies have investigated the use of hybrid colloids for a wide range of purposes such as drug delivery,[6, 7] sensing,[8, 9] photonics,[10] optoelectronics,[11] coatings,[12] and stabilizers.[13]

Hybrid colloids often involve two distinct materials arranged in a core-shell architecture. A variety of techniques have been explored for the development of such core-shell systems, one of which is heteroaggregation.[14] Heteroaggregates are caused by the aggregation of particles with different compositions and/or sizes in colloidal dispersions and have been investigated for use in manufacturing coatings, separations techniques, as well as pharmaceutical devices and biotechnology.[15] Previous methods to produce core-shell heteroaggregates have often relied on ion-pairing to drive heteroaggregation or require covalent grafting of a shell onto a core particle.[16-19] Such methods result in a construct where the core particle is surrounded by a nanoparticle shell, which resembles a raspberry and is often termed a raspberry-like particle (RLP). Various parameters can be used to control the heteroaggregation process. For instance, ion-pair driven heteroaggregation, which relies on electrostatic interactions between the core-particle and the shell particle, is sensitive to pH, ionic strength, and particle sizes. When stimuli-responsive components are used, this offers additional routes to control the rate of heteroaggregation including hydrogen bonding, temperature, or light.[20, 21] Such parameters can even be used to produce reversible heteroaggregation.

ACCEPTED MANUSCRIPT

Heteroaggregates have been constructed from a variety of materials, such as polystyrene/silicon dioxide,[12] polystyrene/iron oxide,[22] polystyrene/poly(2-vinylpyridine),[23] hydroxypropyl cellulose/silica,[19] alginate/$CaCO_3$,[24] and many others. In addition, soft material components have been investigated for the development of RLPs. For example, microgels, which are nano- or micro-scale gel particles, have been investigated for use in heteroaggregation.[23, 25] Using soft, deformable microgels to assemble atop hard sphere "cores" allows for increased contact area; the microgels are able to spread onto the hard spheres, which improves the mechanical stability of the complex.[25] This is beneficial because assembly of heteroaggregates is limited by both the strength of intraparticle bonds and the contact area between the particles. As an example of such soft/hard heteroaggregates, poly(*N*-isopropylacrylamide) (pNIPAm) microgels have been employed due to interest in their thermosensitivity.[15] PNIPAm exhibits a volume phase transition temperature (VPTT) at ~32 °C where it transitions from a swollen gel to a collapsed globular state.[26] PNIPAm microgels have been assembled atop SiO_2 core particles in a number of studies to produce RLPs.[16] Similarly, poly(*N*-isopropylmethacrylamide) (pNIPMAm) based microgels can be used for such systems, with these particles exhibiting a transition temperature at ~41 °C.[26]

The Lyon group has previously reported the synthesis of raspberry-structured microgel heteroaggregates by immersing core particles into a densely packed colloidal (microgel) phase to apply a microgel coating.[27] It is hypothesized that this heteroaggregation occurs due to the amphiphilic nature of pNIPAm and pNIPMAm microgels, making interactions with the amphiphilic polystyrene core possible, even in the case where components possess charges of the same sign. Using this method, we have shown that ultra violet (UV) irradiation can be used to couple the microgels to carboxylated polystyrene (PS) core particles modified with 4-

ACCEPTED MANUSCRIPT

aminobenzophenone (AB). This covalent coupling via UV irradiation is not necessary for the formation of RLPs, but can be employed to enhance stability of the assembly. That study demonstrated the assembly of RLPs using two different microgel compositions (neutral and anionic) and two different core particles (4.5 μm PS and "rough" PS with iron oxide grafted on the surface). Thus, the method allows for versatility in the composition of RLP components, lacking the constraints of ion-pair driven heteroaggregation such as sensitivity to pH and ionic strength. Moreover, since chemical compositional limitiations have not yet been discovered for this system, it can be utilized to interrogate fundamental aspects of microgel deformation at a curved interface.

In the present contribution, we explore the sensitivity of the colloidal-phase mediated heteroaggregation process to the volume fraction of the microgel phase. We have modified the previously described method[27] to enable the creation of colloidal-phases of known volume fractions (**Scheme 1**), thereby obtaining greater control over the packing of microgels around the core particles. Volume fraction is the thermodynamic parameter of interest for colloidal phases.[28] For dispersions of spherical, repulsive hard spheres, the phase diagram predicts a disordered "fluid" phase at sphere volume fractions below 0.49, fluid/crystal coexistence, from 0.49-0.55, and an fcc crystalline phase above 0.55, with the maximal close packing occurring at 0.74. It is also typical to observe a kinetically trapped "glassy" phase with an approximate maximal packing of ~0.64; this glassy phase may coexist with a polycrystalline phase as well. Previous investigations of microgel phase behavior have indicated that microgels behave as hard spheres up to a volume fraction of 0.5.[29] However, above this volume fraction, particle softness begins to influence the phase behavior, leading to a shift in the fluid/crystal phase boundary and a narrowing of the coexistence region.[29] Due to the unique softness of microgels, the parameter

ACCEPTED MANUSCRIPT

volume fraction is often replaced by the effective volume fraction (ϕ_{eff}) according to Equation (1), where *a* represents the average distance between the center of two adjacent microgels, σ represents the microgel hydrodynamic diameter in dilute dispersions, and 0.740 corresponds to the volume fraction for hard sphere closest packing.

$$\phi_{eff} = 0.740(a/\sigma)^3 \qquad \text{Equation (1)}$$

We have also investigated how microgel network structure influences deformation at an interface based on microgel monomer and cross-linker content. Investigation of microgel deformation at planar interfaces has demonstrated the influence of microgel compositions on microgel rigidity and subsequent microgel spreading, leading to varied topographical features. Visual studies of several RLPs comprised of different microgel compositions further elucidate the complex influence microgel structure has on coating efficiency and resulting topography when curved interfaces are introduced to a system. An understandign of these implications could be widely applicable to systems in which microgel deformation occurs on a rigid, curved surface.

Scheme 1. Colloidal-phase mediated heteroaggregation

ACCEPTED MANUSCRIPT

ACCEPTED MANUSCRIPT

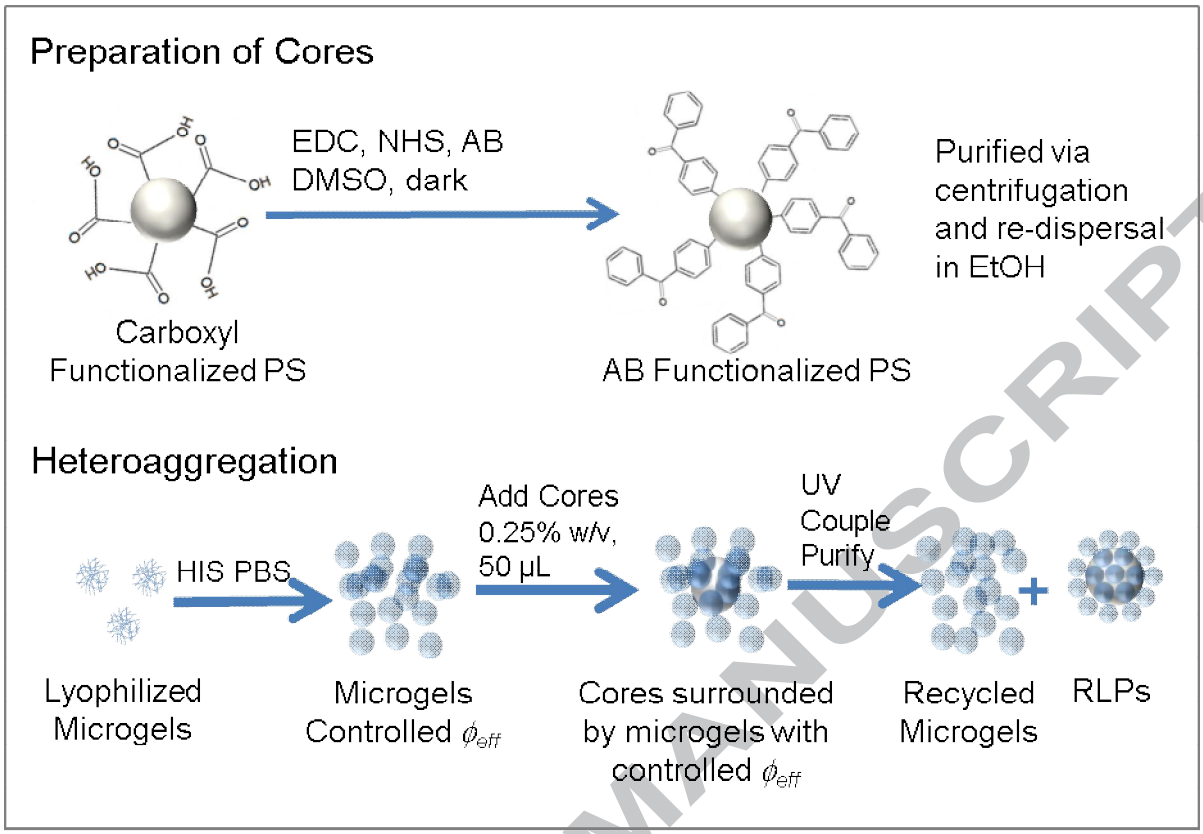

2. Materials and Methods

2.1 Materials

All reagents were purchased from Sigma-Aldrich (St. Louis, MO) and used as received, unless otherwise noted. Reagents *N*,*N*'-methylenebis(acrylamide) (BIS), acrylic acid (AAc), sodium dodecyl sulfate (SDS), ammonium persulfate (APS), 1-ethyl-2-[2-dimethylaminopropyl]carbodiimide hydrochloride (EDC), *N*-hydroxysuccinimide (NHS), 4-aminobenzophenone (AB), ethanol (EtOH), and dimethylsulfoxide (DMSO) were all used as received. The monomers *N*-isopropylacrylamide (NIPAm) and *N*-isopropylmethacrylamide (NIPMAm) were recrystallized from hexanes (VWR international, West Chester, PA) and dried *in vacuo* prior to use. Carboxyl modified polystyrene (PS) spheres were purchased from Polysciences, Inc. (Warrington, PA). Deionized water used in all reactions, purifications, and

ACCEPTED MANUSCRIPT

buffer preparations was purified to a resistance of 18 MΩ (Barnstead E-Pure system), and filtered through a 0.2 μm filter to remove particulate matter.

2.2 Microgel Synthesis

Microgels were synthesized as previously described using precipitation polymerization.[26] For pNIPAm microgels, the total monomer concentration was 100 mM with molar compositions of 95% mol pNIPAm and 5% mol BIS (denoted pNIPAm:BIS (95:5)) or 99% mol pNIPAm and 1% mol BIS (pNIPAm:BIS (99:1)). For samples containing pNIPMAm, the total monomer concentration was 140 mM with molar compositions of either 95% mol pNIPMAm and 5% mol BIS (denoted pNIPMAm:BIS (95:5)) or 99% mol pNIPMAm and 1% mol BIS (pNIPMAm:BIS (99:1)). Monomer, crosslinker, and surfactant SDS were dissolved in water and filtered to remove any undissolved solids. The solution was placed in a 3-neck round bottom flask equipped with a condenser, heated to 70 °C while mixing with a magnetic stir bar (stir speed 450 RPM) while being purged with N_2 for approximately 1 hour. Finally, 1 mL of the initiator APS was added with a syringe needle. A total APS concentration of 1 mM was used for all microgels except the 99% mol pNIPMAm and 1% mol BIS sample, which required an APS concentration of 4 mM to help control microgel size. The solution was held at ~70 °C overnight, and then cooled to room temperature. The microgel solution was filtered through glass wool, purified via sedimentation, and lyophilized for storage.

2.3 Microgel Characterization

Microgel morphological characteristics such as height and spread of individual microgels were determined by passive deposition of dilute solutions of microgels in 10 mM, pH 7.4 phosphate buffer solution (PBS) with 100 mM high ionic strength (HIS) overnight on amine-functionalized silica glass coverslips. These samples were imaged using an MFP-3D Atomic Force Microscope

ACCEPTED MANUSCRIPT

(AFM) system (Asylum Research, Santa Barbara, CA). The parameters associated with 10 microgels were used to determine the average height and spread for each composition. Microgel hydrodynamic radius (R_H) values were determined using a DynaPro Dynamic Light Scattering (DLS) instrument (Wyatt, Technology, Santa Barbara, CA) in high HIS PBS. Viscometry data were obtained using an Ubbelohde viscometer with a viscometer constant of 0.003121 cSt/s at 21 °C. Samples were prepared between 0.05 wt% and 0.35 wt% depending on the microgel composition. Five weight fractions were used for each microgel composition and three trials were performed at each weight fraction. The swelling ratio, *k*, was determined by fitting the data to the Einstein-Batchelor equation as described in the Supporting Information.[30]

2.4 Preparation of Aminobenzophenone-functionalized PS Cores

Before heteroaggregation, core particles were conjugated to AB to enable UV coupling of the core particles to the microgels to add stability to the resulting RLPs (**Scheme 1**). Carboxylated-PS core particles were functionalized with AB (25 mM) via carbodiimide coupling using EDC (2 mM)/NHS (5 mM) in DMSO for two hours in the dark on a shaker. PS core particles were purified in EtOH via ten rounds of sedimentation/resuspension.

2.5 Preparation of Raspberry-Like Particles

RLPs were prepared using colloidal-phase mediated heteroaggregation (**Scheme 1**). For each sample, 5 mg of microgels were dissolved in varied volumes of HIS PBS. AB-functionalized PS core particles were re-suspended in HIS PBS and added to the colloidal phase (0.25% w/v, 50 µL) to produce mixed colloidal dispersions with effective volume fractions between 0.01-0.9. The solutions were homogenized via vortexing after which the samples were exposed to longwave UV rays from a Blak Ray 100 W lamp for 30 minutes. Samples were purified via sequential sedimentation and resuspension in EtOH.

ACCEPTED MANUSCRIPT

2.6 Characterization of Raspberry-Like Particles

Microparticles were imaged using a NOVA 200 Focused Ion Beam/ Scanning Electron Microscope system (FEI, Hillsboro, OR) to assess the resulting RLP microgel coverage. Samples were prepared by placing a drop of purified microparticles dispersed in EtOH on copper tape adhered to a metal stub. The samples were coated with gold/palladium for 2-3 minutes at 25 V using a Hummer V Sputterer (Anatech USA, Union City, CA). Semi-quantitative characterization of the mean diameter of the RLPs was performed using a qNano particle analyzer (iZON, Oxford, United Kingdom) with a 4000 nm pore. Measurements were made in filtered 10 mM formate buffer of pH 3.3 and ionic strength of 10 mM. Voltage and pressure values were set to optimize the signal to ensure high sensitivity. Controlling the voltage setting ensures that the current is in a range where blockade events can be resolved. Increased pressure is often necessary to ensure that particles translocate at an appropriate rate without clogging the pore. The voltage was set to either 0.16 V for PS core samples and pNIPAm RLP samples or 0.20 V for pNIPMAm samples. The pressure was set to either 10 cm H_2O for PS samples and pNIPAm samples or 15 cm H_2O for pNIPMAm RLP samples. The pore was set to a stretch of 49 mm for all samples. The measurements were calibrated using the provided 4050 nm latex standard. For each sample, three trials were analyzed via qNano.

2.7 Statistical Analysis of qNano Translocation Data

Due to the nature of these microparticles and the qNano, large particle aggregates (diameter > 3σ of each sample set) were removed prior to statistical analysis. All statistical analyses for qNano translocation studies were performed with InStat (GraphPad, San Diego CA). Average particle diameter data were statistically analyzed using one-way analysis of variance using the Tukey-Kramer multiple comparisons test at a 95% confidence interval (n = 3000 particles).

ACCEPTED MANUSCRIPT

3. Results and Discussion

3.1 Determination of Microgel Structure and Properties

Microgels were prepared using either pNIPAm or pNIPMAm as the main comonomer to determine whether the microgel composition, and hence morphology, influence the heteroaggregation process. Two concentrations (1% mol or 5% mol) of the crosslinker *N,N'*-methylenebis(acrylamide) (BIS) were used to determine the influence of particle stiffness on the heteroaggregation process. Previous studies in our group have revealed that the microgel network structure is dictated by the monomer of choice.[31] PNIPAm particles typically have a heterogeneous cross-linker distribution, resulting in a dense core surrounded by a loose corona of dangling chains. In contrast, pNIPMAm particles have been demonstrated to have a more homogenous network structure with cross-linking uniformly distributed throughout the entire particle domain. Indeed, the differences in particle morphology can be seen via AFM when evaluating the height of free standing microgels that have been passively deposited (**Table 1**, **Figure 1**, and **Figure S1**). AFM characterization indicates that pNIPAm microgels are more deformable than pNIPMAm microgels, having significantly smaller heights upon deformation than do the pNIPMAm microgels, which suggests structural dissimilarities. Moreover, pNIPAm microgels also have k-value scaling parameters as determined by viscometry compared to their pNIPMAm counterparts, which indicates that the pNIPAm microgels are able to swell to a higher degree than the pNIPMAm microgels; the k-value is a scaling parameter that provides an indication of volume fraction occupied by a swollen particle. We also investigated two cross-linker contents for both pNIPAm and pNIPMAm microgels to determine the influence of particle rigidity on this heteroaggregation process. Higher cross-linker contents lead to larger heights determined via AFM and smaller k-value parameters determined via viscometry (**Table 1**). A

ACCEPTED MANUSCRIPT

detailed explanation of the viscometry data analysis required to determine the k-value parameters can be found in the Supporting Information (**Figure S2**).

Table 1. Microgel Characterization

Monomer and Crosslinker Molar Ratio		**Spread / nm**	**Height / nm**	**R_H / nm**	**k-value/ mL-mg^{-1}**
pNIPAm:BIS	99:1	986 ± 31	17 ± 1	233 ± 3	24 ± 1
pNIPAm:BIS	95:5	560 ± 24	52 ± 8	254 ± 6	15 ± 1
pNIPMAm:BIS	99:1	935 ± 47	31 ± 2	399 ± 4	21 ± 1
pNIPMAm:BIS	95:5	585 ± 20	98 ± 6	288 ± 3	10 ± 1

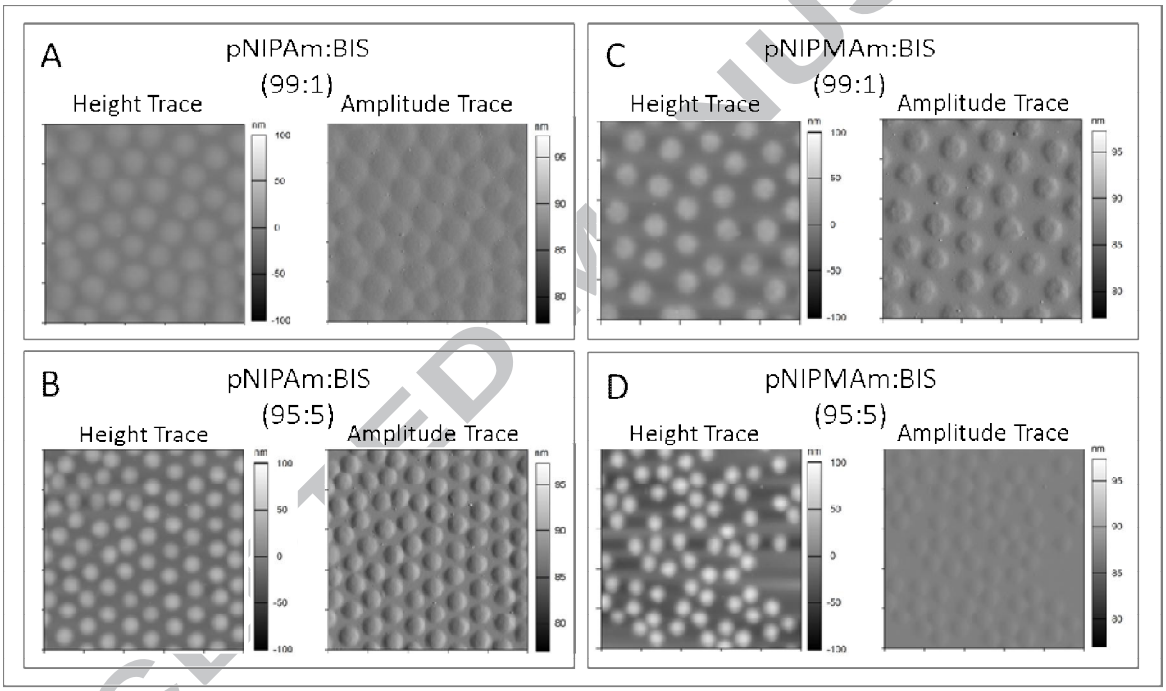

Figure 1. AFM images of passively deposited microgel samples onto APTMS-functionalized coverslips. The height trace and amplitude trace of all four samples: (A) pNIPAm:BIS (99:1), (B) pNIPAm:BIS (95:5), (C) pNIPMAm:BIS (99:1), and (D) pNIPMAm:BIS (95:5). All images are 5 μm x 5 μm scans.

3.2 Qualitative Evaluation of Raspberry-Like Particle Coverage

ACCEPTED MANUSCRIPT

Heteroaggregation was evaluated at a range of effective volume fractions to determine the influence on the resulting microgel coverage of the RLP. Analysis of SEM imaging suggests that the ability of microgels to spread is a critical factor in determining the degree of coating success to form an RLP via colloidal-phase mediated heteroaggregation. SEM imaging (**Figure 2**) indicates that the pNIPAm:BIS (99:1) microgels are able to spread and coat the surface at all effective volume fractions with little variation in the degree of coverage. The pNIPAm:BIS (95:5) microgels similarly are able to spread and cover the surface at all effective volume fractions; however, the coverage is notably patchier at the highest effective volume fraction of 0.8. Thus, the microgel cross-linker content and colloidal phase effective volume fraction appear to have a limited influence on the resulting microgel coverage of the pNIPAm RLPs.

ACCEPTED MANUSCRIPT

ACCEPTED MANUSCRIPT

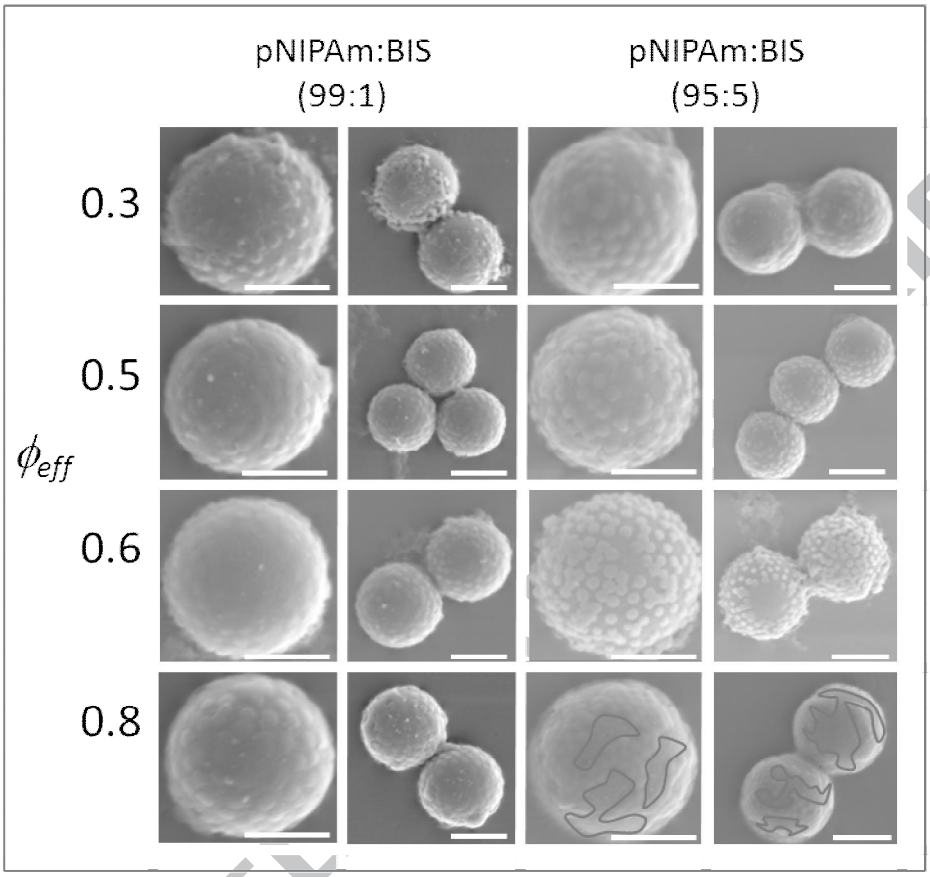

Figure 2. Representative SEM images for pNIPAm RLPs produced at varying effective volume fractions indicate a high degree of microgel coverage for all samples. Samples are coated with gold/palladium prior to imaging. In the sample at $\phi = 0.8$, areas devoid of microgels are outlined in grey. All scale bars are 2 μm.

In contrast, SEM imaging of pNIPMAm RLPs (**Figure 3**) suggests that the heteroaggregation process is highly dependent on effective volume fraction when using pNIPMAm microgels. The pNIPMAm:BIS (99:1) microgels are able to coat more effectively at

ACCEPTED MANUSCRIPT

higher effective volume fractions (ϕ_{eff} = 0.6 and 0.8). However, at effective volume fractions corresponding to the hard sphere fluid (ϕ_{eff} = 0.3) and coexistence (ϕ_{eff} = 0.5) phases, very few microgels can be found on the surface of the resulting RLPs. In contrast, the pNIPMAm:BIS (95:5) microgels are most successful at coating the PS core at the lowest effective volume fraction (ϕ_{eff} = 0.3) corresponding to the fluid phase. As the effective volume fraction of the colloidal phase is increased, the coating appears to become irregular and less consistent from particle to particle. This irregularity of the microgel coating is likely caused by unfavorable energetics that inhibit deformation of the microgels at the hard PS interface. Here we see not only a strong dependence on effective volume fraction, but also a strong influence of the microgel stiffness. Heteroaggregation was assessed at a larger range of effective volume fractions for all microgels and imaged via SEM (**Figure S3 and Figure S4**). The appearance of the pNIPAm and pNIPMAm RLPs via SEM imaging are strikingly dissimilar (**Figure 2** and **Figure 3**) due to different modes of microgel deswelling that occur during drying. The pNIPAm microgels, which are more deformable are capable of undergoing anisotropic deswelling, regardless of cross-linker content. In contrast, pNIPMAm microgel are not as easily deformed and would favor isotropic deswelling particularly when the network is further constrained by a high cross-linker content, as we see in the sample at ϕ_{eff} = 0.3 (**Figure 3**).

ACCEPTED MANUSCRIPT

ACCEPTED MANUSCRIPT

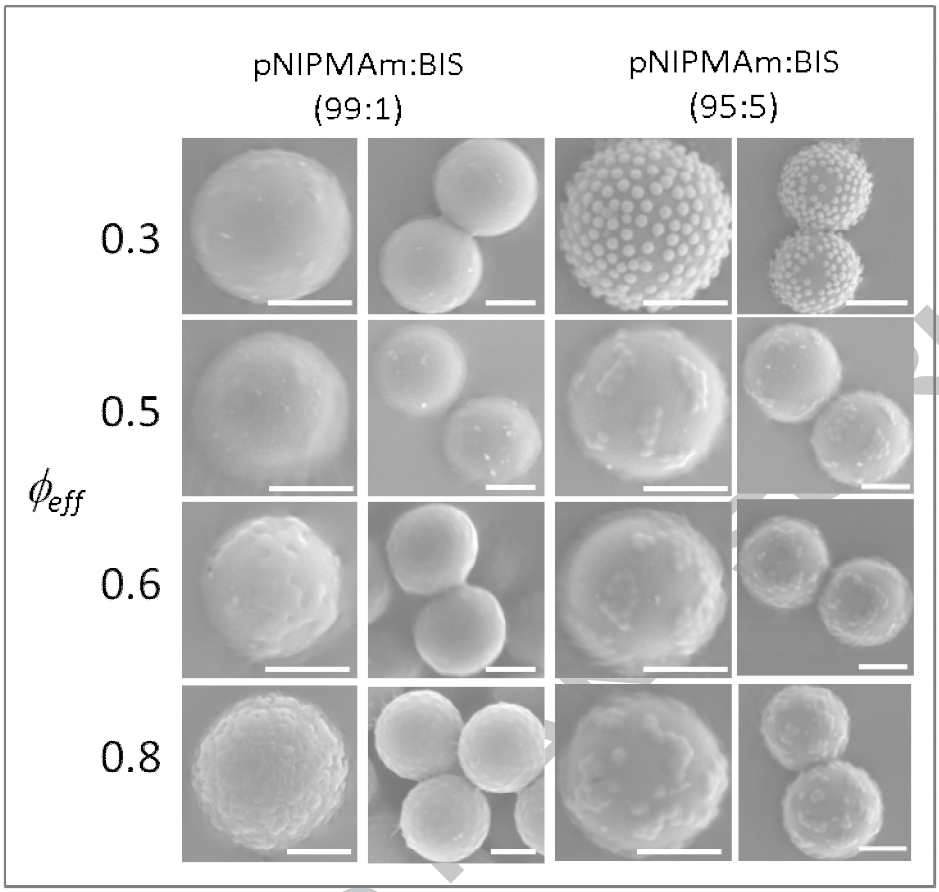

Figure 3. Representative SEM images for pNIPMAm RLPs produced at varying effective volume fraction demonstrate that this process is highly dependent on effective volume fraction of the colloidal phase. Samples are coated with gold/palladium prior to imaging. All scale bars are 2 μm.

This method consistently produces homogeneously coated RLPs when using soft, deformable pNIPAm microgels. In contrast, denser, more rigid pNIPMam microgels are more sensitivite to effective volume fraction of the colloidal phase for successful heteroaggregation. The influence of microgel stiffness on coating coverage and topography seen in characterization studies on planar surfaces is likely magnified upon introduction of a curved interface, which requires increased network deformation. The influence of microgel stiffness on colloidal-phase mediated heteroaggregation can likely be attributed to the energy required to deform the

ACCEPTED MANUSCRIPT

microgel at the interface of a PS core particle. The loose pNIPAm microgel network allows for facile deformation of the dangling polymer chains of the microgel, enabling these microgels to greatly deform at the PS interface and separate from the colloidal phase. In contrast, the denser, more uniform pNIPMAm microgel network requires a higher energy input to deform the entire microgel network at the PS interface to separate out of the colloidal phase. This deformation process is likely energetically unfavorable, resulting in a more sensitive heteroaggregation process that can be easily disturbed by parameters such as the cross-linker content and the effective volume fraction.

The relationship between microgel cross-linker content and effective volume fractions for successful heteroaggregation is not yet well understood. The microgel stiffness could be influencing the structure and fluidity of the colloidal phase during this process. Previous investigators have demonstrated that pNIPAm microgel softness can cause changes in colloidal-phase behavior and cause shifting in the phase boundaries.[29] However, pNIPMAm microgel phase behavior has received markedly less investigation in this context. Such microgels, which show inherent structural differences, may exhibit widely different phase behavior that is influencing this heteroaggregation process.

3.3 Semi-Quantitative Evaluation of Raspberry-Like Particle Coverage

3.3.1 Evaluation of Increase in Particle Diameter

Next, we investigated the use of the qNano particle analyzer as a means for a semi-quantitative, high-throughput technique to analyze the resulting microgel coverage of the RLPs. The qNano particle analyzer relies on tunable resistive pulse sensing. This technique monitors the current flow through an aperture (in this case a pore in an elastomeric sheet), while also allowing for a tunable aperture size via stretching of the pore. Individual particles can be

ACCEPTED MANUSCRIPT

detected while they pass through the pore as a change in the ionic current flow (blockade event). The amplitude of such a blockade, known as the blockade magnitude, is indicative of the particle size. Using this instrument, we were able to determine the mean RLP diameters (**Figure 4**) and the size distribution, as inferred from the translocation behavior through a pore of specified size (4000 nm with a 49 mm stretch in all cases for this work). The pNIPAm:BIS (99:1) RLPs exhibit mean diameters that are significantly larger ($p < 0.001$) than the bare PS cores. Additionally, for these samples, RLP mean diameters are significantly different from RLP samples at most other effective volume fractions. However, the comparison of RLP samples at $\phi_{eff} = 0.6$ and $\phi_{eff} = 0.8$ show no significant difference in mean diameter. The pNIPAm:BIS (95:5) RLPs also exhibit significantly larger ($p < 0.001$) mean diameters as compared to the bare PS cores. These mean diameters are also significantly different ($p < 0.001$) as compared to RLPs produced at other effective volume fractions with the exception of the comparison of RLPs produced at $\phi_{eff} = 0.3$ and $\phi_{eff} = 0.8$.

The pNIPMAm:BIS (99:1) RLPs exhibit mean RLP diameters that are more similar to the PS cores for two effective volume fractions: 4370 ± 140 nm ($\phi_{eff} = 0.5$) and 4370 ± 80 nm ($\phi_{eff} = 0.8$). RLPs are significantly smaller ($p < 0.001$) for $\phi_{eff} = 0.3$ (4220 ± 60 nm) and significantly larger ($p < 0.001$) for $\phi_{eff} = 0.6$ (4650 ± 30 nm). In addition, RLP samples at different ϕ_{eff} are significantly different ($p < 0.001$) except for the comparison of samples fabricated at $\phi_{eff} = 0.5$ and $\phi_{eff} = 0.8$. The pNIPMAm:BIS (99:5) RLPs also exhibit varied mean diameters depending on the effective volume fraction. We observe mean RLP diameters that are significantly larger ($p < 0.001$) than the bare PS cores only in the case of $\phi_{eff} = 0.3$ where the mean diameter is 4470 ± 40 nm. We observe mean RLP diameters that are significantly smaller ($p < 0.001$) than the bare PS cores for $\phi_{eff} = 0.5$ (4050 ± 90 nm), $\phi_{eff} = 0.6$ (4220 ± 60 nm), and

ACCEPTED MANUSCRIPT

ϕ_{eff} = 0.8 (4090 ± 30 nm). Additionally, RLP samples at different ϕ_{eff} are significantly different ($p < 0.001$) for all comparisons except for RLPs fabricated at ϕ_{eff} = 0.5 compared to those fabricated at ϕ_{eff} = 0.8. For the case of both the pNIPMAm microgel RLPs, several RLP samples exhibit mean diameters that are smaller than the PS cores, which could suggest the presence of unpurified microgel aggregates. Overall, for most cases the standard deviations for three trials are relatively small, indicating that this heteroaggregation coating process is reproducible. However, these data provide us with little information about the heterogeneity of the resulting RLP populations.

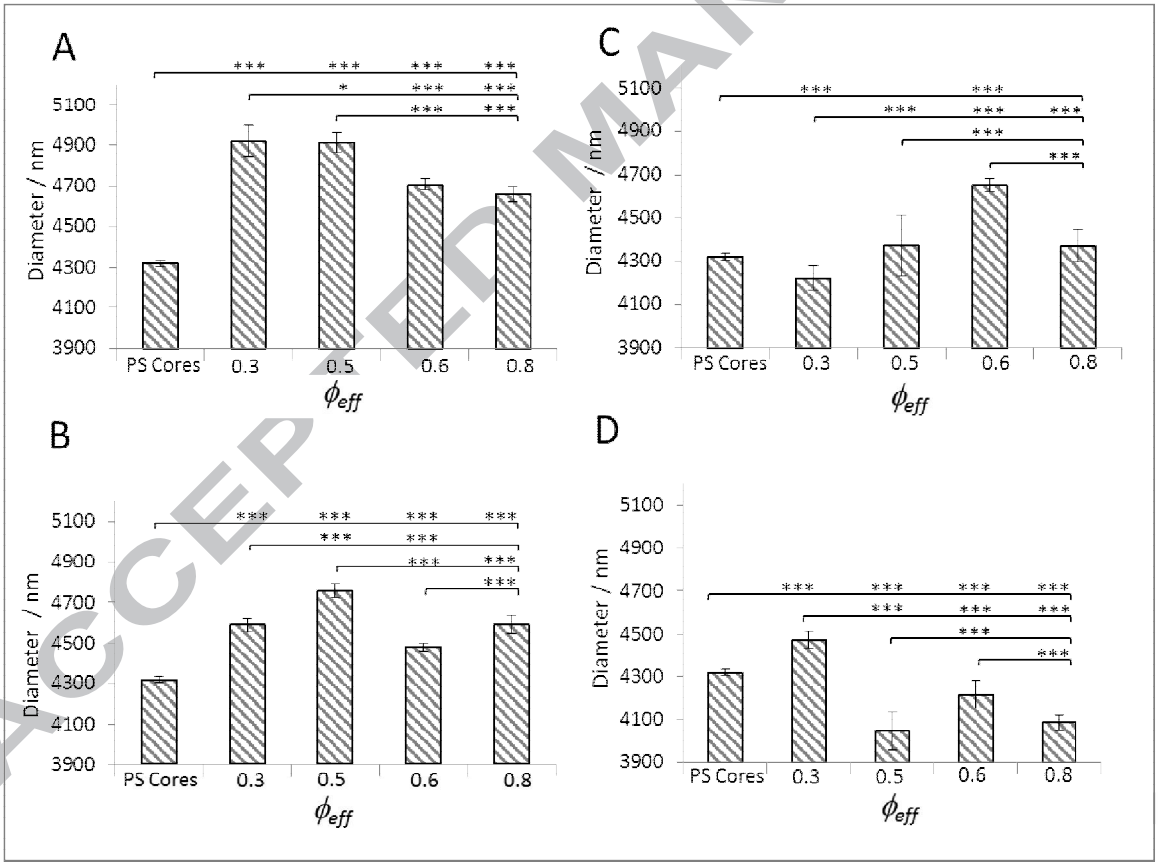

Figure 4. qNano particle counter mean RLP diameter for three trials of (A) pNIPAm:BIS (99:1) RLPs, (B) pNIPAm:BIS (95:5) RLPs, (C) pNIPMAm:BIS (99:1) RLPs, and (D) pNIPMAm:BIS

ACCEPTED MANUSCRIPT

(95:5) RLPs. Error bars represent the standard deviation between three trials of 1000 particle blockade events. The p-values are indicates by asterisks where * indicates $p < 0.05$ and *** indicates $p < 0.001$.

3.3.2 Evaluation of Particle Diameter Histograms

We also analyzed particle diameter information in a histogram format for enhanced visualization of the data (**Figure 5, Figure 6, Figure 7,** and **Figure 8**). Comparison between RLP samples synthesized with the same microgel population can provide information about the efficiency of the coating process because of the nature of the qNano measurements. The resistive pulse sensing technique is influenced by the degree of microgel coverage for individual RLPs, providing an average particle diameter (**Scheme 2**). A particle with low microgel coverage will still have a measured diameter that is larger than the PS core alone because the swollen microgels will cause a slight increase in the magnitude of the blockade. As the microgel coverage is increased, the blockade magnitude, and particle diameter, will increase until a maximum is reached when the RLP exhibits full microgel coverage. Thus, the largest peak shifts within a given RLP composition suggest the highest coating efficiency while smaller peak shifts suggest lower coating efficiencies. However, such comparisons between RLP populations composed of different microgels would not provide much insight into the coating efficiencies because different microgels have different swelling behaviors. Analysis of the distribution curve width can provide useful information about the homogeneity of the RLP population.

Scheme 2. Factors influencing qNano determination of diameter

ACCEPTED MANUSCRIPT

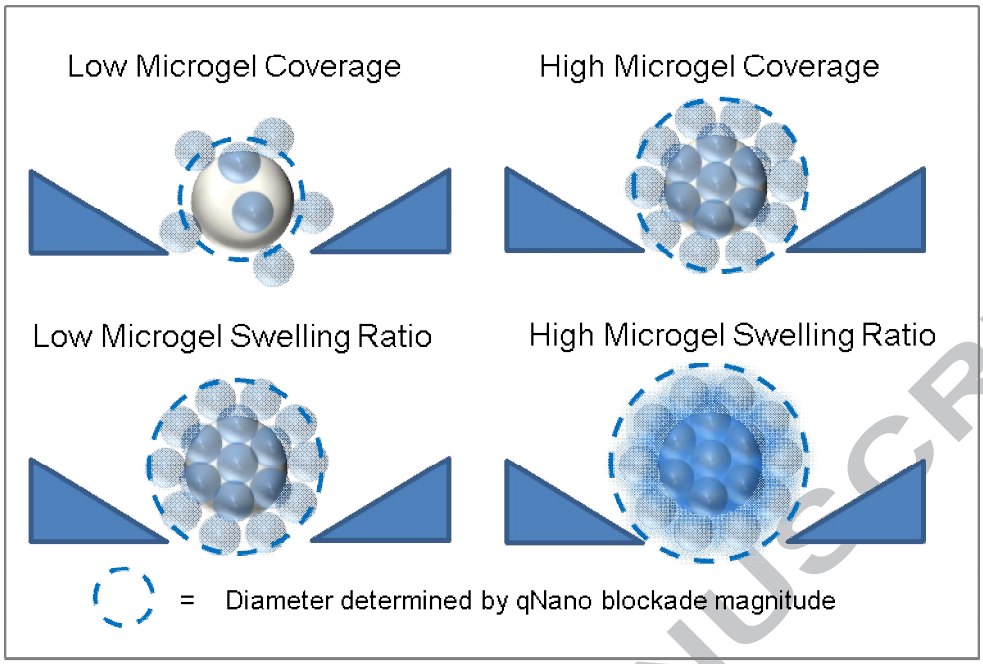

PNIPAm:BIS (99:1) RLPs exhibit a peak shift for all effective volume fractions in comparison to the PS core particles (**Figure 5**). For ϕ_{eff} = 0.3 and 0.5, the RLPs exhibit large peak shifts (~450 nm) with a constant distribution width (~1500 nm). Such a shift in the entire distribution curve indicates that a constant microgel shell thickness has been added to all PS cores, suggesting that the resulting RLP population has a homogenous coating. For the higher values of ϕ_{eff} = 0.6 and 0.8, the peak shift is less pronounced (~300 nm) with a narrower distribution width (~1300 nm) as compared to the PS cores (~1500 nm). A narrowing of the distribution width provides us with little informataion on the heterogeneity of the samples. However, it is possible that the narrowing of this distribution curve is caused by multiple populations of RLPs that have different degrees of microgel coatings; for instance, smaller core particles could be fully coated while larger core particles may be partially coated. The RLPs constructed using pNIPAm:BIS (95:5) exhibit a smaller peak shift in all cases (~300 nm), which is likely caused by the greater stiffness (and decreased swelling) of the microgels due to the

ACCEPTED MANUSCRIPT

higher percent of the cross-linker, BIS (**Figure 6**). For these samples, the width of the peak is similar to that of the PS cores, suggesting the presence of a homogeneously coated population of RLPs. Tails in the distributions at larger sizes suggest the presence of a small population of RLP aggregates.

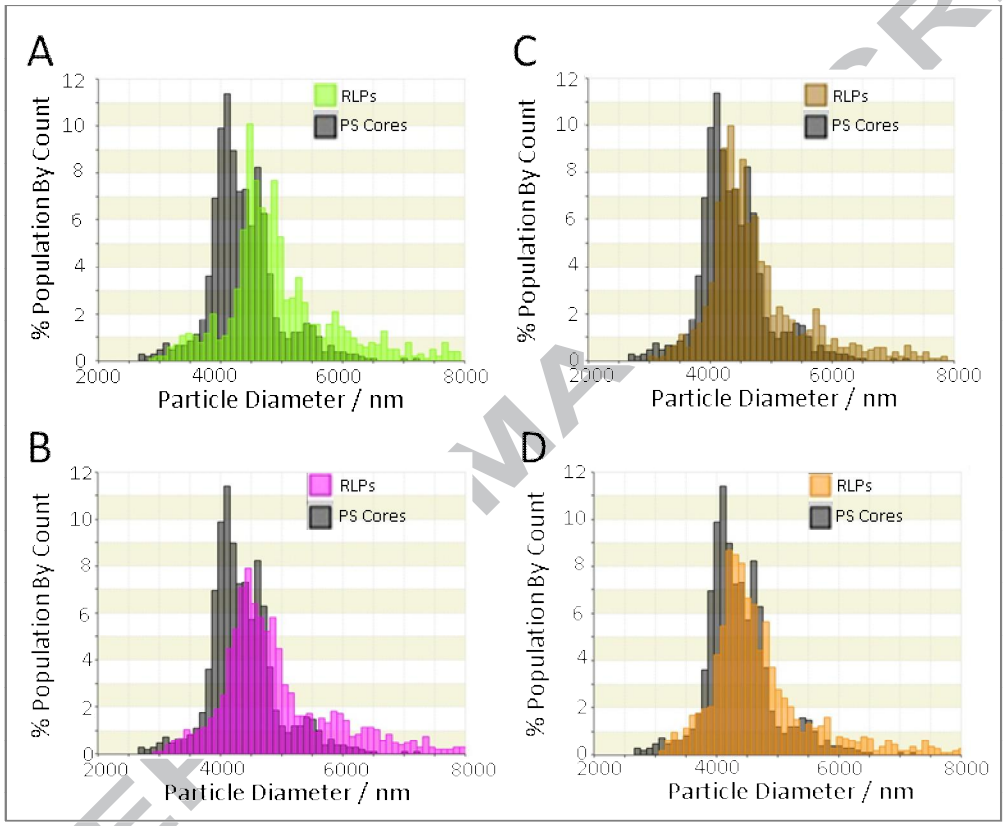

Figure 5. qNano particle diameter representative histograms for pNIPAm:BIS (99:1) RLPs at (A) ϕ_{eff} = 0.3, (B) ϕ_{eff} = 0.5, (C) ϕ_{eff} = 0.6, and (D) ϕ_{eff} = 0.8. RLP and PS Cores data were collected using a 4000 nm pore at an applied stretch of 49 mm, an applied pressure setting of 10 cm H_2O, and a voltage setting of 0.16 V. All samples were calibrated using the provided 4050 nm latex standards.

ACCEPTED MANUSCRIPT

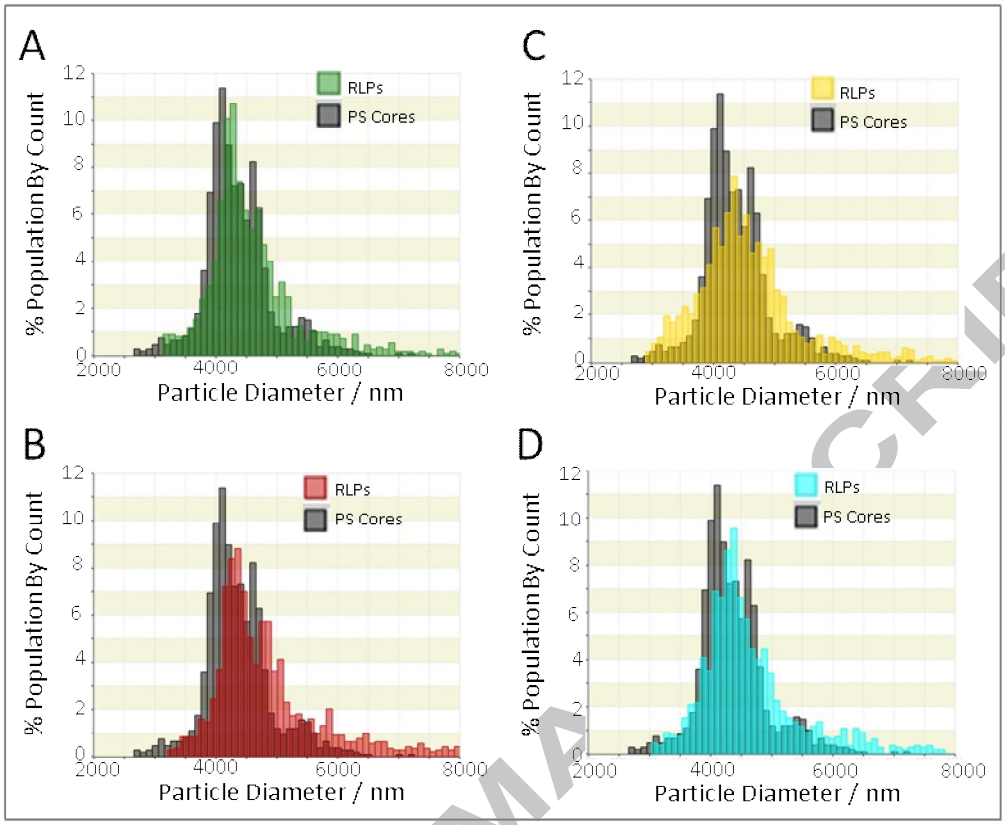

Figure 6. qNano particle diameter representative histograms for pNIPAm:BIS (95:5) RLPs at (A) ϕ_{eff} = 0.3, (B) ϕ_{eff} = 0.5, (C) ϕ_{eff} = 0.6, and (D) ϕ_{eff} = 0.8. RLP and PS Cores data were collected using a 4000 nm pore at an applied stretch of 49 mm, an applied pressure of 10 cm H_2O, and a voltage setting of 0.16 V. All samples were calibrated using the provided 4050 nm latex standards.

The pNIPMAm:BIS (99:1) RLPs exhibit a slight peak shift (~200 nm) at ϕ_{eff} = 0.3 and 0.5 (**Figure 7A** and **Figure 7B**). However, the entire distribution curve does not shift with the peak. At ϕ_{eff} = 0.6 and ϕ_{eff} = 0.8, these RLPs exhibit larger peak shifts (~325 nm) with little difference in the distribution curve width in comparison to the PS cores, suggesting the presence of homogeneously coated RLPs (**Figure 7C** and **Figure 7D**). These RLP samples also have a larger population of smaller particles, which are likely caused by microgel aggregates. In

ACCEPTED MANUSCRIPT

contrast, the pNIPMAm:BIS (95:5) RLPs do not exhibit appreciable curve shifts (**Figure 8**). These RLP samples also exhibit larger populations of smaller particles, again likely due to the presence of microgel impurities.

Interestingly, for the pNIPMAm:BIS (95:5) sample, although the ϕ_{eff} = 0.3 sample exhibits a significant increase in mean RLP diameter ($p > 0.001$), the histogram shows little variation between the RLP sample and the PS core sample. This could be attributed to the denser, more rigid pNIPMAm microgel network structure. Stiffer microgels are limited in their ability to deform, leading to reducing spreading on the core surface. Once coupled to the core, stiffer microgels are also limited in their ability to swell, which directly influences the blockade magnitude measured by the qNano. Microgels that exhibit a higher degree of swelling likely produce a thicker coating in the swollen state (**Scheme 2**), causing a larger blockade magnitude that results in a greater difference in mean diameter of the RLP as compared to the bare PS cores. For microgels that exhibit less swelling, the blockade magnitude is smaller, resulting in a smaller difference in particle mean diameter before and after heteroaggregation. These data suggest a minimum swelling percentage must be achieved by the microgels for a marked peak shift to occur via qNano.

ACCEPTED MANUSCRIPT

ACCEPTED MANUSCRIPT

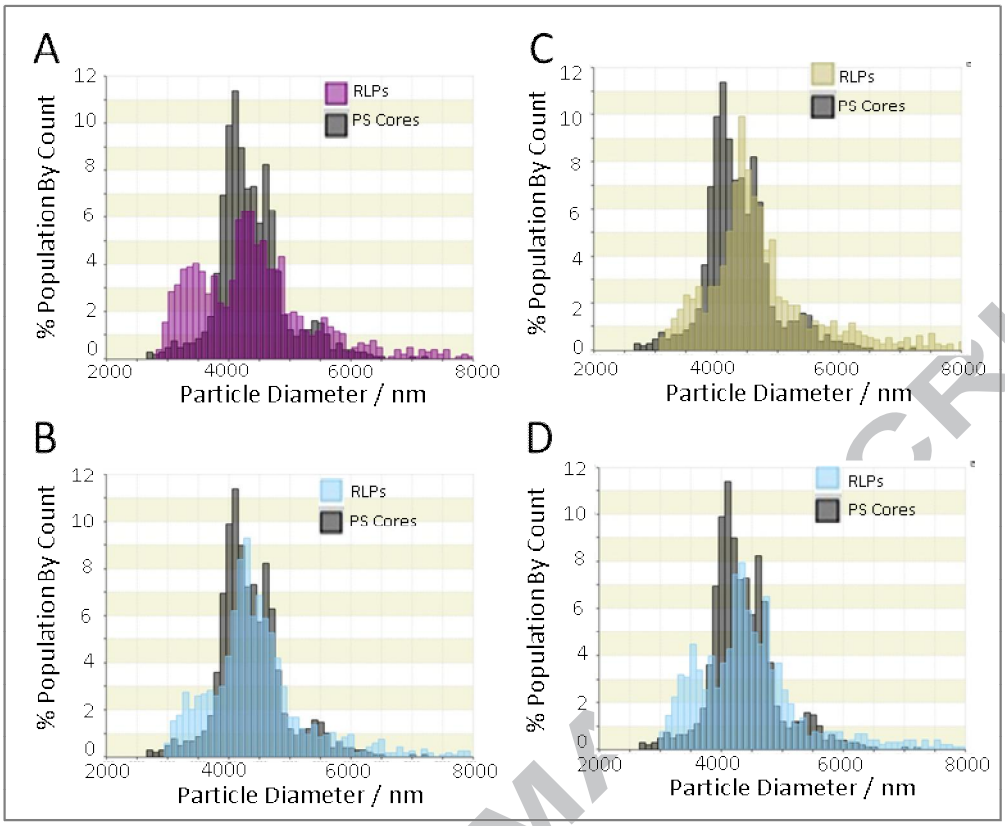

Figure 7. qNano particle diameter representative histograms for pNIPMAm:BIS (99:1) RLPs at (A) ϕ_{eff} = 0.3, (B) ϕ_{eff} = 0.5, (C) ϕ_{eff} = 0.6, and (D) ϕ_{eff} = 0.8. RLP data were collected using a 4000 nm pore at an applied stretch of 49 mm, an applied pressure setting of 15 cm H_2O, and a voltage setting of 0.20 V. PS Cores data were collected using a 4000 nm pore at an applied stretch of 49 mm, an applied pressure setting of 10 cm H_2O, and a voltage setting of 0.16 V. All samples were calibrated using the provided 4050 nm latex standard.

ACCEPTED MANUSCRIPT

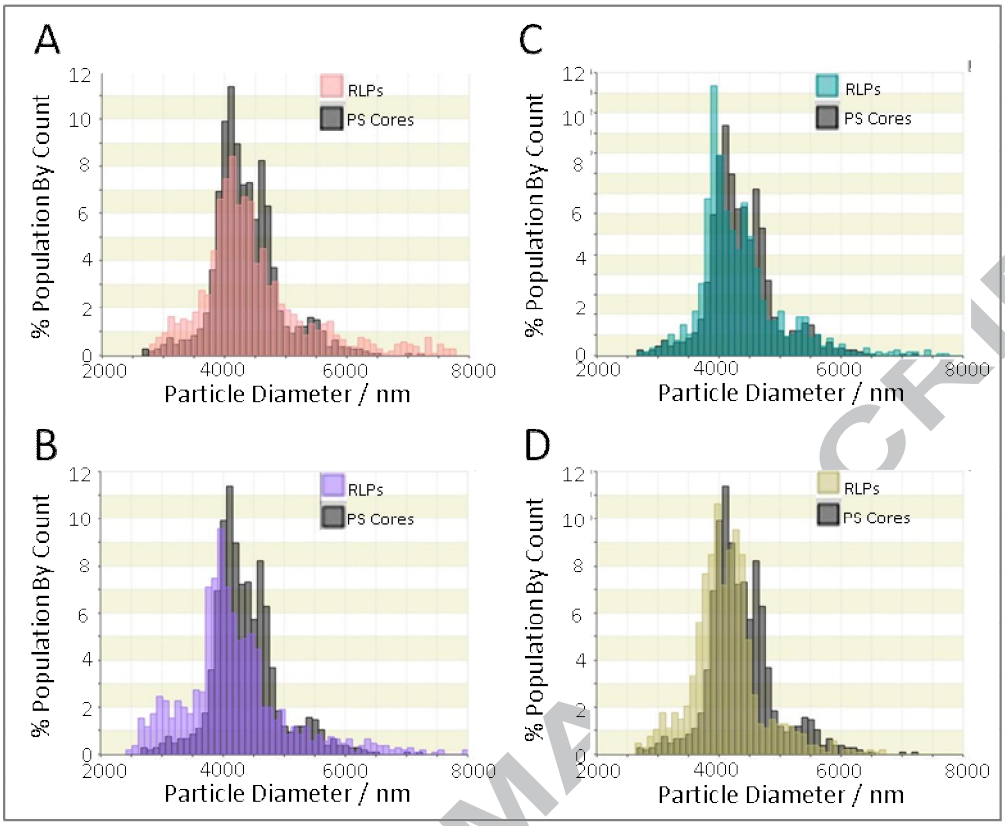

Figure 8. qNano particle diameter representative histograms for pNIPMAm:BIS (95:5) RLPs at (A) ϕ_{eff} = 0.3, (B) ϕ_{eff} = 0.5, (C) ϕ_{eff} = 0.6, and (D) ϕ_{eff} = 0.8. RLP data were collected using a 4000 nm pore at an applied stretch of 49 mm, an applied pressure setting of 15 cm H_2O, and a voltage setting of 0.20 V. PS Cores data were collected using a 4000 nm pore at an applied stretch of 49 mm, an applied pressure setting of 10 cm H_2O, and a voltage setting of 0.16 V. All samples were calibrated using the provided 4050 nm latex standard.

Comparison of the qNano translocation data to the SEM images suggests that the qNano may be an effective, high-throughput analysis tool to determine the presence of a microgel coating on a core particle after heteroaggregation when both the mean diameters of the samples and the histograms are analyzed. For each microgel composition, the RLP mean diameter data aligns with the SEM images, except in the case of pNIPMAm:BIS (99:1) at ϕ_{eff} = 0.8. In this

ACCEPTED MANUSCRIPT

case, the mean RLP diameter found by the qNano particle translocation analysis indicates that the microgel coverage is limited; yet, SEM images indicate the presence of homogeneously coated RLPs (**Figure 3**). Analysis of the qNano histogram (**Figure 7**) indicates the presence of a microgel population that remains after purification, leading to a lowered mean diameter; additionally, the peak shift (~325 nm) of the entire distribution curve indicates the presence of a homogeneously coated RLP population. Analysis of both the qNano RLP mean diameter and histograms provide information on several aspects of the RLP population obtained from this heteroaggregation process including reproducibility, coating efficiency, heterogeneity of the microgel coating, and the presence of microgel impurities. However, the use of the qNano is limited in its ability to ascertain information about subtleties in the RLP topography that are more clearly seen via SEM image analysis such as microgel spreading at the interface and spacing of microgels.

Analysis of qNano translocation data suggests that success of this technique in determining RLP microgel coverage is influenced by the ability of the microgels to swell. Indeed pNIPAm:BIS (99:1) microgels, which demonstrate the highest degree of swelling in PBS, as indicated by the largest k-value scaling parameter (24 ± 1), produce RLPs that exhibit the largest peak shifts (~450 nm) (**Figure 5**). Furthermore, when the cross-linker content is increased and the pNIPAm:BIS (95:5) microgels are used, the k-value scaling parameter decreases (15 ± 1) as does the peak shift exhibited by the RLPs (~300 nm), even though SEM imaging indicates that both pNIPAm microgels are able to form well-coated RLPs at all effective volume fractions (**Figure 2** and **Figure 6**). In this case, the qNano measurements do indicate the presence of a microgel coating that is not as thick as in the case of the pNIPAm:BIS (99:1) RLPs. Since these microgels have very similar hydrodynamic radii (**Table 1**), we would expect a resulting coating

ACCEPTED MANUSCRIPT

of similar thickness and thus a similar peak shift if microgel swelling were not influencing the detection. Analysis of pNIPMAm microgel RLPs further supports this conclusion. The pNIPMAm microgels have smaller k-value scaling parameters than the pNIPAm microgel (pNIPMAm:BIS (99:1) ~ 21 ± 1 and pNIPMAm:BIS (95:5) ~ 10 ± 1). Though the pNIPMAm:BIS (99:1) microgels exhibit a peak shift (~325 nm) at ϕ_{eff} = 0.6 and ϕ_{eff} = 0.8, corresponding to well-coated RLPs via SEM image analysis, it is markedly smaller than those produced by the corresponding pNIPAM:BIS (99:1) RLPs (**Figure 3** and **Figure 7**). Moreover, RLPs constructed using pNIPMAm:BIS (95:5) microgels do not exhibit an appreciable peak shift even at ϕ_{eff} = 0.3 (**Figure 8**) where SEM image analysis and qNano mean RLP diameter data confirm the presence of a microgel coating. The lack of a peak shift is likely caused by the inability of these microgels to swell to an appreciable extent due to their greater rigidity as demonstrated by their small k-value scaling parameter (10 ± 1). Taken together, analysis of qNano mean diameter data and histograms of diameters can be used to determine success of RLP coatings. In cases where excess microgel populations exist, purification processes can be modified and success can be analyzed via qNano histograms. Upon elimination or reduction of microgel aggregates, mean diameter data can be used to identify populations of well-coated RLPs. However, it is likely that when microgels of vastly different compositions are used, SEM imaging may be required to qualitatively calibrate initial qNano results.

4. Conclusion

We have assessed the influence of microgel composition and colloidal-phase volume fraction on colloidal-phase mediated heteroaggregation. Though pNIPAm microgels have a relatively high coating affinity regardless of cross-linker content or colloidal-phase volume fraction, pNIPMAm microgels are much more sensitive to these parameters. This difference is likely caused by the inherent structural dissimilarities between the two microgel types, which

ACCEPTED MANUSCRIPT

influence the amount of energy required for deformation to occur at the curved PS interface. PNIPAm microgels are easily deformed at an interface, likely requiring little energy input for deformation to occur; as such, they are an ideal candidate for colloidal-phase mediated heteroaggregation with a non-deformable core particle. In contrast, pNIPMAm microgels do not deform as easily as pNIPAm microgels, likely due to unfavorable energetics, resulting in a more sensitive coating process that is further limited upon increased stiffness. These coating behaviors are likely magnified due to the increased deformation that must occur at a curved interface. An understanding of microgel deformation at a curved interface can be widely applicable to other systems such as pickering emulsions[32, 33] and colloidosomes.[34, 35]

Gaining insight into the influence that the colloidal-phase volume fraction and the microgel composition have on this heteroaggregation process enables us to use this method to develop a platform of complex stimuli-responsive microparticles with few compositional restraints. Through comparison of SEM imaging and qNano translocation events, we have demonstrated that the qNano can be used in the future as a high-throughput analysis method to gain information regarding the coating efficiency, homogeneity of the population, and purity of samples. Further comparison of qNano data provided as mean diameters versus histograms can even provide insight into properties of the microgels such as the ability to swell. In this manner, the use of such a high-throughput analysis technique will enable us to develop a platform of RLPs for use in a variety of applications.

Acknowledgements

Funding for SS was provided by NSF (2736B48) and the NSF Integrative Graduate Education and Research Traineeship program in Stem Cell Biomanufacturing (0965945).

References

ACCEPTED MANUSCRIPT

[1] Zhang, M. F.; Breiner, T.; Mori, H.; Muller, A. H. E., *Polymer* **2003,** *44,* 1449.
[2] Cong, Y.; Xia, T.; Zou, M.; Li, Z. N.; Peng, B.; Guo, D. Z.; Deng, Z. W., *J. Mat. Chem. B* **2014,** *2,* 3450.
[3] Zhang, S. W.; Zhou, S. X.; Weng, Y. M.; Wu, L. M., *Langmuir* **2005,** *21,* 2124.
[4] Caruso, F.; Spasova, M.; Saigueirino-Maceira, V.; Liz-Marzan, L. M., *Adv. Mater.* **2001,** *13,* 1090.
[5] Zhou, S. G.; McIlwrath, K.; Jackson, G.; Eichhorn, B., *J. Am. Chem. Soc.* **2006,** *128,* 1780.
[6] Park, S.; Park, H. H.; Kim, S. Y.; Kim, S. J.; Woo, K.; Ko, G., *Appl. Environ. Microbiol.* **2014,** *80,* 2343.
[7] Wu, K. H.; Liu, C. I.; Yang, C. C.; Wang, G. P.; Chao, C. M., *Mater. Chem. Phys.* **2011,** *125,* 802.
[8] Zhang, J.; Ma, N.; Tang, F.; Cui, Q.; He, F.; Li, L., *ACS Appl. Mater. Interfaces* **2012,** *4,* 1747.
[9] Mansur, A.; Mansur, H.; Gonzalez, J., *Sensors* **2011,** *11,* 9951.
[10] Ohnuma, A.; Cho, E. C.; Jiang, M.; Ohtani, B.; Xia, Y., *Langmuir* **2009,** *25,* 13880.
[11] Perro, A.; Reculusa, S.; Ravaine, S.; Bourgeat-Lami, E. B.; Duguet, E., *J. Mater. Chem.* **2005,** *15,* 3745.
[12] Qian, Z.; Zhang, Z. C.; Song, L. Y.; Liu, H. R., *J. Mater. Chem.* **2009,** *19,* 1297.
[13] Fujii, S.; Yokoyama, Y.; Miyanari, Y.; Shiono, T.; Ito, M.; Yusa, S.; Nakamura, Y., *Langmuir* **2013,** *29,* 5457.
[14] Islam, A. M.; Chowdhry, B. Z.; Snowden, M. J., *Adv. Colloid Interface Sci.* **1995,** *62* 109.
[15] Bradley, M.; Lazim, A. M.; Eastoe, J., *Polymers* **2011,** *3,* 1036.
[16] Dechezelles, J. F.; Malik, V.; Crassous, J. J.; Schurtenberger, P., *Soft Matter* **2013,** *9,* 2798.
[17] Harley, S.; Thompson, D. W.; Vincent, B., *Colloids Surf.* **1992,** *62,* 163.
[18] Luckham, P.; Vincent, B.; Hart, C. A.; Tadros, T. F., *Colloids Surf.* **1980,** *1,* 281.
[19] Furusawa, K.; Anzai, C., *Colloids Surf.***1992,** *63,* 103.
[20] Starck, P.; Ducker, W. A., *Langmuir* **2009,** *25,* 2114.
[21] Plunkett, K. N.; Mohraz, A.; Haasch, R. T.; Lewis, J. A.; Moore, J. S., *J. Am. Chem. Soc.* **2005,** *127,* 14574.
[22] Lu, Z. Y.; Qin, Y. Q.; Fang, J. Y.; Sun, J.; Li, J.; Liu, F. Q.; Yang, A. S., *Nanotechnology* **2008,** *19,1*.
[23] Snoswell, D. R. E.; Rogers, T. J.; Howe, A. M.; Vincent, B., *Langmuir* **2005,** *21,* 11439.
[24] Liu, H.; Wang, C.; Gao, Q.; Liu, X.; Tong, Z., *Int. J. Pharm.* **2008,** *351,* 104.
[25] Snoswell, D. R. E.; Brill, R. K.; Vincent, B., *Adv. Mater.* **2007,** *19,* 1523.
[26] Hendrickson, G. R.; Smith, M. H.; South, A. B.; Lyon, L. A., *Adv. Funct. Mater.* **2010,** *20,* 1697.
[27] Gaulding, J. C.; Saxena, S.; Montanari, D. E.; Lyon, L. A., *Acs Macro Lett.* **2013,** *2,* 337.
[28] Smith, R. K.; Lewis, P. A.; Weiss, P. S., *Prog. Surf. Sci.* **2004,** *75,* 1.
[29] Senff, H.; Richtering, W., *J. Chem. Phys.* **1999,** *111,* 1705.
[30] Borrega, R.; Cloitre, M.; Betremieux, I.; Ernst, B.; Leibler, L., Europhysical Lett.1999, 47, 729.
[31] Smith, M. H.; Herman, E. S.; Lyon, L. A., *J. Phys. Chem. B.* **2011,** *115,* 3761-3764.
[32] Ramsden,W. *Proc. R. Soc. London.* **1903**, 72, 156.

ACCEPTED MANUSCRIPT

[33] Pickering, S.U. *J. Chem. Soc.* **1907**, 91, 2001.
[34] Kim, J.W.; Fernandez-Nieves, A.; Dan, N.; Utada, A.S.; Marquez, M.; Weitz, D.A. *Nano Lett.* **2007**, 7, 2876.
[35] Lawrence, D.B.; Cai, T.; Hu, Z.; Marquz, M.; Dinsmore, A.D. *Langmuir*, **2007**, 23, 395

List of Captions

Scheme 1. Colloidal-phase mediated heteroaggregation

Scheme 2. Factors influencing qNano determination of diameter

Table 1. Microgel Characterization

Figure 1. AFM images of passively deposited microgel samples onto APTMS-functionalized coverslips. The height trace and amplitude trace of all four samples: (A) pNIPAm:BIS (99:1), (B) pNIPAm:BIS (95:5), (C) pNIPMAm:BIS (99:1), and (D) pNIPMAm:BIS (95:5). All images are 5 μm x 5 μm scans.

Figure 2. Representative SEM images for pNIPAm RLPs produced at varying effective volume fractions indicate a high degree of microgel coverage for all samples. Samples are coated with gold/palladium prior to imaging. All scale bars are 2 μm.

Figure 3. Representative SEM images for pNIPMAm RLPs produced at varying effective volume fraction demonstrate that this process is highly dependent on effective volume fraction of the colloidal phase. Samples are coated with gold/palladium prior to imaging. All scale bars are 2 μm.

ACCEPTED MANUSCRIPT

Figure 4. qNano particle counter mean RLP diameter for three trials of (A) pNIPAm:BIS (99:1) RLPs, (B) pNIPAm:BIS (95:5) RLPs, (C) pNIPMAm:BIS (99:1) RLPs, and (D) pNIPMAm:BIS (95:5) RLPs. Error bars represent the standard deviation between three trials of 1000 particle blockade events. The p-values are indicates by asterisks where * indicates $p < 0.05$ and *** indicates $p < 0.001$.

Figure 5. qNano particle diameter representative histograms for pNIPAm:BIS (99:1) RLPs at (A) $\phi_{eff} = 0.3$, (B) $\phi_{eff} = 0.5$, (C) $\phi_{eff} = 0.6$, and (D) $\phi_{eff} = 0.8$. RLP and PS Cores data were collected using a 4000 nm pore at an applied stretch of 49 mm, an applied pressure setting of 10 cm H_2O, and a voltage setting of 0.16 V. All samples were calibrated using the provided 4050 nm latex standards.

Figure 6. qNano particle diameter representative histograms for pNIPAm:BIS (95:5) RLPs at (A) $\phi_{eff} = 0.3$, (B) $\phi_{eff} = 0.5$, (C) $\phi_{eff} = 0.6$, and (D) $\phi_{eff} = 0.8$. RLP and PS Cores data were collected using a 4000 nm pore at an applied stretch of 49 mm, an applied pressure of 10 cm H_2O, and a voltage setting of 0.16 V. All samples were calibrated using the provided 4050 nm latex standards.

Figure 7. qNano particle diameter representative histograms for pNIPMAm:BIS (99:1) RLPs at (A) $\phi_{eff} = 0.3$, (B) $\phi_{eff} = 0.5$, (C) $\phi_{eff} = 0.6$, and (D) $\phi_{eff} = 0.8$. RLP data were collected using a 4000 nm pore at an applied stretch of 49 mm, an applied pressure setting of 15 cm H_2O, and a voltage setting of 0.20 V. PS Cores data were collected using a 4000 nm pore at an applied

ACCEPTED MANUSCRIPT

stretch of 49 mm, an applied pressure setting of 10 cm H_2O, and a voltage setting of 0.16 V. All samples were calibrated using the provided 4050 nm latex standard.

Figure 8. qNano particle diameter representative histograms for pNIPMAm:BIS (95:5) RLPs at (A) ϕ_{eff} = 0.3, (B) ϕ_{eff} = 0.5, (C) ϕ_{eff} = 0.6, and (D) ϕ_{eff} = 0.8. RLP data were collected using a 4000 nm pore at an applied stretch of 49 mm, an applied pressure setting of 15 cm H_2O, and a voltage setting of 0.20 V. PS Cores data were collected using a 4000 nm pore at an applied stretch of 49 mm, an applied pressure setting of 10 cm H_2O, and a voltage setting of 0.16 V. All samples were calibrated using the provided 4050 nm latex standard.

Supplementary Information Figures

Figure S1. Representative AFM height traces of individual microgels deposited via passive deposition onto APTMS-functionalized glass coverslips: (A) pNIPAm:BIS (99:1), (B) pNIPAm:BIS (95:5), (C) pNIPMAm:BIS (99:1), (C) pNIPMAm:BIS (95:5).

Figure S2. Viscometry data for (A) pNIPAm:BIS (99:1), (B) pNIPAm:BIS (95:5), (C) pNIPMAm:BIS (99:1), (D) and pNIPMAm:BIS (95:5). Data points represent the average of three trials. Error bars represent the standard deviation of three trials.

Figure S3. Representative SEM images of pNIPAm:BIS microgel RLPs at varying effective volume fractions. All scale bars are 2 μm.

ACCEPTED MANUSCRIPT

Figure S4. Representative SEM images of pNIPMAm:BIS microgel RLPs at varying effective volume fractions. All scale bars are 2 μm.

List of Tables

Table 1. Microgel Characterization

Monomer and Crosslinker Molar Ratio		**Spread / nm**	**Height / nm**	**R_H / nm**	**k-value / mL-mg^{-1}**
pNIPAm:BIS	99:1	986 ± 31	17 ± 1	233 ± 3	24 ± 1
pNIPAm:BIS	95:5	560 ± 24	52 ± 8	254 ± 6	15 ± 1
pNIPMAm:BIS	99:1	935 ± 47	31 ± 2	399 ± 4	21 ± 1
pNIPMAm:BIS	95:5	585 ± 20	98 ± 6	288 ± 3	10 ± 1

ACCEPTED MANUSCRIPT

ACCEPTED MANUSCRIPT

Graphical Abstract

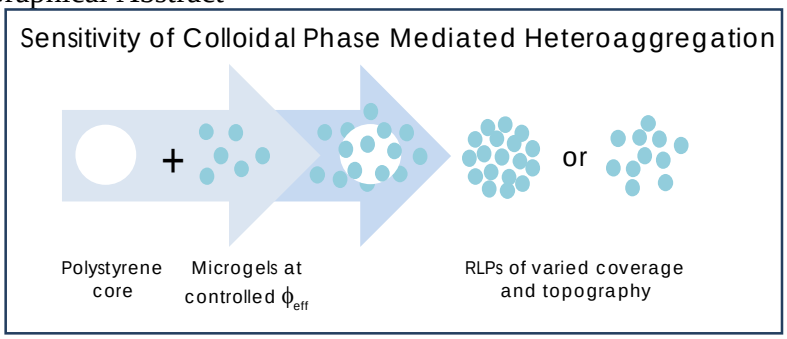

ACCEPTED MANUSCRIPT

ACCEPTED MANUSCRIPT

Highlights

- Microgel structure and colloidal phase influence heteroaggregation
- Deformation at a curved interface is dependent on the polymer network structure
- qNano resistive-pulse sensing can be used for high throughput analysis of RLPs

ACCEPTED MANUSCRIPT